Faraday Discussions

Cite this: DOI: 10.1039/d5fd00003c

PAPER

Asymmetric phase transitions in lipid bilayers: coupling or bending?†

Mona Krompers,[a] Miriam Jaki,[a] Sinja Götz,[a] Jan Lembeck,[a] Laurine Kaul,[a] Martin Holzer[a] and Heiko Heerklotz *[abc]

Received 8th January 2025, Accepted 15th January 2025
DOI: 10.1039/d5fd00003c

Biomembranes show asymmetric lipid composition of their two leaflets. The phenomenon that ordered domains in one leaflet may affect the order of the other has been referred to as interleaflet coupling and discussed in terms of transmembrane signaling. Many coupling mechanisms have been proposed; one potential mechanism should arise from the fact that the isolated melting of an ordered, *e.g.*, gel phase gives rise to a significant expansion of this leaflet, resulting in a mismatch between the intrinsic areas of the leaflets. This asymmetry stress can be accommodated in a number of ways. One is interleaflet coupling – individually higher- and lower-melting leaflets melt together at intermediate melting temperature. Alternatively, the membrane may bend towards the larger-intrinsic-area leaflet, bud and release very small daughter vesicles (DVs). Here, we prepared lipid-asymmetric large unilamellar vesicles (aLUVs) with low-melting stearyl-oleyl-phosphatidylcholine (SOPC) in the inner and SOPC with ~20 mol% of high-melting dipalmitoyl phosphatidylglycerol (DPPG) in the outer leaflet. Phase transitions in aLUVs *versus* LUVs were recorded with pressure perturbation calorimetry; vesicle budding was monitored by asymmetric flow field-flow fractionation (AF4) and visualized by cryo-transmission electron microscopy. An HPLC protocol was established to quantify the total DPPG content; zeta potential was used to detect outer-leaflet DPPG. It turned out to be possible to prepare aLUVs at 5 and 15 °C, with the outer leaflet partially in the gel phase. The properties of the final aLUVs depended on the preparation temperature. aLUVs prepared at 5 and 15 °C caused the budding of exovesicles upon heating and only weak coupling of the phase transitions of the leaflets. aLUVs prepared at 30 °C with both leaflets in the fluid state showed stronger coupling upon asymmetric freezing/melting at lower temperature. This is in line with the hypotheses that (i) the exchange of lipid between close-to lipid-saturated cyclodextrin and acceptor vesicles at a given temperature results in largely stress-free bilayers and (ii) that outside budding and coupling are, to some extent, alternative responses of the bilayer to asymmetric expansion. These hypotheses help explaining

[a]*Department of Pharmaceutics, University of Freiburg, Institute of Pharmaceutical Sciences, Freiburg, Germany. E-mail: heiko.heerklotz@pharmazie.uni-freiburg.de*
[b]*University of Toronto, Leslie Dan Faculty of Pharmacy, Toronto, Canada*
[c]*BIOSS Center for Biological Signaling Studies, Freiburg, Germany*

† Electronic supplementary information (ESI) available. See DOI: https://doi.org/10.1039/d5fd00003c

our and some literature data; the overall understanding and prediction of coupling for any given aLUV system remains an urgent, open question.

Introduction

Recently, the effects of lipid asymmetry on the function of biological membranes and the roles of membrane intrinsic-area asymmetry stress in biological membrane remodeling phenomena have been attracting much interest. The study presented here considers the interplay between lipid species asymmetry and intrinsic-area asymmetry.

The intrinsic area of a lipid leaflet depends on the number of lipids and their optimal lateral area, at which repulsive and attractive interactions match at least in-plane.[1] Thereby, intrinsic areas of different molecules are not necessarily additive as illustrated impressively by the lipid-condensing effect of cholesterol.[2–4] Furthermore, even at the intrinsic area per molecule, *i.e.*, at zero lateral force within the interfacial plane, residual out-of-plane forces give rise to an intrinsic leaflet curvature.[5]

A mismatch between the intrinsic areas of two attached leaflets, also referred to as intrinsic-area asymmetry, asymmetry stress, differential stress, or bilayer spontaneous curvature, induces a tendency to bend the bilayer.[6] A straightforward way to study asymmetry stress effects in vesicular model systems and cells in detail is to insert or extract membrane-impermeant molecules to or from the accessible, outer leaflet. This can be achieved with membrane-partitioning yet impermeant lipopeptides,[7,8] lysolipids[9,10] and other surfactants.[11,12] Their addition to vesicles causes positive asymmetry stress, *i.e.*, overpopulation of the outer compared to the inner leaflet. Extraction from rather relaxed, surfactant-containing membranes, for example by dilution, induces negative asymmetry stress. The analogous approach has been demonstrated for phospholipids with the help of cyclodextrins able to solubilize lipids in the extravesicular solution.[13] Whereas "empty" cyclodextrin extracts lipid from the outer leaflet, oversaturated (supercooled) cyclodextrin–lipid complexes overpopulate it. The approaches using soluble and cyclodextrin-solubilized amphiphiles have revealed strong analogies.

A primary response to asymmetry stress is membrane bending, causing membrane shape changes and tubulation or budding and fission of daughter vesicles (DVs).[10,13–16] The extent to which these phenomena are possible can be increased by hypertonic conditions increasing the area-per-volume ratio of the membrane.[10,13] As bending effects reach their limit, one or more alternative asymmetry-stress responses kick in.[16] The fact that the activity of a lipid or surfactant in a membrane leaflet is increased in an overpopulated and reduced in an underpopulated leaflet[9,13,17] can, at some point, repel membrane-partitioning molecules into aqueous solution.[9,17,18] The linked leaflet may adjust by a gradual change of the area per lipid within a given phase[19,20] or by an enforced formation of a more condensed or ordered phase,[13] respectively. Lipid flip-flop, usually taking of the order of days, can be accelerated to occur within minutes.[21] Finally, asymmetry stress by surfactant insertion or lipid extraction may reach a threshold for transient membrane failure or even the collapse of the vesicle altogether.[13,17,22,23]

Asymmetry stress can also result from different thermal expansion of the leaflets in lipid-asymmetric membrane – the direct representation of Sheetz and Singer's[6] bimetallic couple analogy. Overpopulation, *i.e.*, increased lateral pressure can condense lipids into a gel phase well above its melting temperature, T_m, in symmetrical membranes.[13] Analogously, the melting-induced expansion in a low-T_m leaflet should stretch an opposed, high-T_m leaflet and may melt its lipid. In other words, asymmetric melting or formation of gel phase induces asymmetry stress and asymmetry stress should be a strong coupling mechanism of transitions in the two leaflets if it cannot be relaxed otherwise.

In fact, the coupling between transitions between ordered (*e.g.*, gel, liquid ordered) and fluid phase or state in one leaflet with the properties of the opposed leaflet of the bilayer has attracted much interest, also as a potential transmembrane signaling event. Evidence for such coupling has been found in large and giant liposomes[19,24–28] as well as in planar, supported or free-standing membranes.[29–31] Coupling effects have been found for some of the asymmetric membrane compositions investigated, mostly using scanning calorimetry or using fluorescent probes detecting membrane order. Several mechanisms have been proposed for coupling of membrane ordering transitions or changes and, in turn, the registration of ordered domains in the two leaflets. These include headgroup electrostatics, intrinsic lipid curvature, chain interdigitation, cholesterol flip-flop, or differential stress between two leaflets.[26,32–34] Interleaflet coupling is known to induce domain formation[35] and affect lateral lipid diffusion.[36] See Table S9 in ESI† for a more comprehensive overview of contributions. Overall, the effects governing interleaflet coupling appear to be so complex that in spite of a good basis of data, it seems still impossible to predict, for a chosen asymmetric vesicle, whether it shows strong, weak, or virtually no coupling of order-inducing or -reducing transitions between the leaflets.

The current study aims to elucidate whether asymmetric area changes cause coupling and or bending in vesicles of SOPC in the inner and 80 mol% SOPC + 20 mol% DPPG in the outer leaflet, in short, $SOPC^{in}|+20\%\ DPPG^{out}$ or without specification of the specific fraction of DPPG added, $SOPC^{in}|+DPPG^{out}$. This is done by detecting both bending (*i.e.*, outward budding of DVs) *via* AF4 and interleaflet coupling of the gel–fluid transition by differential scanning (DSC) and pressure perturbation calorimetry (PPC).

Furthermore, we will test the hypothesis that the lipid exchange between outer leaflet and largely saturated lipid-loaded cyclodextrin complexes produces rather relaxed, asymmetry-stress-free liposomes.[37,38] Of course, the range of suitable cyclodextrin and loaded-lipid concentrations must be limited – cyclodextrin with no or very little lipid will extract and lipid-supersaturated cyclodextrin will insert lipid, leading to negative and positive asymmetry stress, respectively.[13] However, there seems to be a substantial range in between these extremes where lipid exchange with cyclodextrin causes very little asymmetry stress.[37] This hypothesis would imply that the properties of aLUVs prepared at identical concentrations and, hence, with essentially equal outer and inner leaflet compositions would differ in their properties depending on the exchange temperature they have been prepared at. Tackling this question requires the preparation of aLUV also under exchange conditions where all or part of the membrane is in the gel phase. It remains to be shown whether this usually avoided procedure is feasible in the first place.

Specifically, we will test the suitability of the aLUV protocol that had been introduced for POPC^{in}|+20–50 mol% POPG^{out} [37,38] for vesicles of SOPC^{in}|+20 mol% DPPG^{out}. To this end, a novel HPLC protocol was set up to quantify DPPG. Transition temperatures for pure, symmetrical vesicles are 41.3 °C for DPPG[39] and about 5 °C for SOPC (see Marsh[40] for a compilation). The exchange will be done at 30 °C, where all lipids are fluid as well as at 15 °C and 5 °C, when the outer or both leaflets shall partially be in the gel phase. That means, at 15 °C, aLUVs will be disordered^{in}|ordered^{out}, also referred to as DI/OO in the literature. If the exchange really causes essentially asymmetry-stress-free liposomes, significant stress should build up as, after cyclodextrin removal, the temperature is changed and lipids melt and expand primarily in the outer leaflet. The phase transitions were monitored by DSC and PPC. The latter has the advantage to equilibrate and then probe heats of pressure increase and decrease at each temperature point instead of scanning, allowing for measurements at as little as 2 °C and for minimizing and revealing hysteresis effects.

Budding of exovesicles has been considered a possible response to asymmetry stress but not observed to accompany asymmetric phase transitions so far. The problem is that changes in vesicle size distribution have been monitored by dynamic light scattering which must fail to detect such effects. If, for example, "mother" vesicles are 130 nm in diameter and 20% of the lipid resides in DVs of 20 nm size, the latter will contribute only $(20/130)^4 = 0.3\%$ to the scattered light intensity. The fourth power describes the ratio between sphere surface, which correlates with the amount of lipid, and scattered light intensity. In other words, DLS is principally blind to vesicle budding. Here, budding of DVs will be tested by AF4, a technique detecting size distributions after separating the differently sized particles with incorporated fluorescent lipid (1 mol% NBD-DSPE). This way, it succeeds in characterizing vesicle budding as demonstrated upon addition of lysolipids recently.[10,16] Here, it reported the formation of small particles upon phase transitions that were confirmed to be very small DVs vesicles by cryo-TEM.

Materials and methods

Materials

1,2-Dipalmitoyl-*sn*-glycero-3-phospho-*rac*-glycerol sodium salt (DPPG-Na) was kindly contributed by Lipoid (Ludwigshafen, Germany). 1-Stearoyl-2-oleoyl-*sn*-glycero-3-phosphocholine (SOPC) and 1,2-distearoyl-*sn*-glycero-3-phosphoethanolamine-*N*-(7-nitro-2-1,3-benzoxadiazol-4-yl) ammonium salt (NBD-DSPE) were purchased from Avanti Polar Lipids (Alabaster, US). Randomly methylated β-cyclodextrin (mβCD) (>98%), sodium azide (NaN_3), sodium chloride (NaCl) and ammonium acetate (>99%) were purchased from Sigma-Aldrich (St. Louis, MO, US) and Vivaspin Turbo 4 centrifugal filters (4 mL; MWCO 100 kDa) were obtained from Sartorius (Stonehouse, UK). Ethylenediaminetetraacetic acid (EDTA; ≥99%) and tris(hydroxymethyl)aminomethane (Tris; ≥99.9%), and acetic acid (100%) were purchased from Carl Roth GmbH (Karlsruhe, Germany). Methanol (HPLC ULTRA LC-MS grade; ≥99.9%) was obtained from VWR International (Leuven, Belgium). Purified water was derived from an in-house arium pro water purification system from Sartorius AG (Göttingen, Germany). All other chemicals were purchased from Carl Roth (Karlsruhe, Germany) and were of analytical grade.

Vesicle preparation

Large unilamellar vesicles (LUVs) of SOPC were prepared according to standard procedures.[41,42] In brief, lipids or lipid mixtures dissolved in chloroform or chloroform/methanol (2 : 1) were dried using a rotational vacuum concentrator (Martin Christ, Osterode am Harz, DE) to a thin film and further under a high vacuum overnight. For AF4 experiments, 1 mol% of fluorescent lipid (NBD-DSPE) was incorporated into the film. The lipid film was rehydrated with buffer (110 mM NaCl, 10 mM Tris, and 0.5 mM EDTA at pH 7.4). After five freeze–thaw-cycles, the lipid dispersion was extruded 21 times through an 80 nm nucleopore track-etch polycarbonate membrane (Whatman, Maidstone, UK) at 25 °C using a LipoFast extruder (Avestin, Ottawa, Canada). Multi-lamellar vesicles (MLVs) composed of DPPG were prepared in the same way but were not extruded. The phospholipid concentration was determined by Bartlett Assay,[43] and the integrity of LUVs by dynamic light scattering (DLS).

Preparation of asymmetric liposomes

aLUVs were prepared as described previously.[37,38] Briefly, 1.0 mL of 5 mM SOPC liposomes with ~20 mol% DPPG in the outer leaflet was prepared in two steps: first, 15 mM DPPG liposomes were completely disintegrated and the lipid complexed by adding 150 mM mβCD at 50 °C. Second, LUVs of ~40 mM SOPC were prepared to serve as "acceptor" vesicles. Donor complexes and acceptor vesicles were brought to the desired exchange temperature (5, 15 or 30 °C) and then mixed to produce an incubation mixture containing a total of 5 mM SOPC, 0.63 mM DPPG and 50 mM mβCD. Standard incubation was carried out in a thermomixer at 1000 rpm for 20 minutes – spot checks for validation were done with longer incubation times as shown below.

After preparation, free mβCD and lipid–mβCD complexes were eliminated from the aLUV dispersion by centrifugation through Vivaspin Turbo 4 centrifugal filters, diluting the mβCD below a calculated value of <0.5 mM. The resulting DPPG content in the outer leaflet was quantified by ζ-potential measurements using a calibration curve provided as Fig. S3 in the ESI.† To prepare scrambled liposomes, aLUVs were dried under vacuum, the lipids re-dissolved in 0.5 mL chloroform/methanol (2 : 1) and dried again to obtain a lipid film, followed by rehydration and extrusion as described above.

Dynamic light scattering (DLS) and ζ

A Zetasizer Nano ZS (Malvern, Worcestershire, UK) equipped with a 633 nm He–Ne laser was used to measure particle size distributions as well as the ζ-potential of LUVs and aLUVs. Three measurements at 25 °C were taken for hydrodynamic diameter, polydispersity index (PDI), and ζ-potential for each sample. Effects of viscosity and refractive index of buffer components were taken into account. DLS was performed to confirm the intensity-weighted hydrodynamic diameter to be around 100 nm and the polydispersity index (PDI) to be ≤0.1. The sample was measured in a 4 mL polystyrene cuvette with a layer thickness of 10 mm (Sarstedt AG & Co. KG, Nümbrecht, Germany) at a detection angle of 173°. For ζ-potential measurements a flow-through, high-concentration ζ-potential cell (HCC; Malvern, UK) was used, as described before.[37] A transfer standard (ZTS1240, Malvern)

with a specification of -40 ± 6 mV was measured at the beginning and end of each set of experiments to assess the quality of the setup. Liposomal dispersions were diluted to 1 mM prior to ζ-potential measurements.

Differential scanning calorimetry (DSC) and pressure perturbation calorimetry (PPC)

A VP-DSC (Malvern Instruments, Inc., Northampton, NC, USA) was used.[44] The sample cell was loaded with liposomes dispersed in buffer, while the reference cell was filled with plain buffer. Concerning DSC, samples were scanned from 2–45 °C at a scan rate of 20 K h^{-1}, and the heating power required for the desired temperature increase was measured. Data analysis with MicroCal Origin provided the apparent temperature-dependent molar heat capacity of the lipid vesicles, C_p. PPC measurements were performed as described previously.[45] In brief, the thermal volume expansion was determined by measuring the heat response to an isothermal pressure perturbation in a VP-DSC operating in isothermal mode (high gain, low noise mode). Pressure jumps between 5.3 bar and ambient were applied to a thermally equilibrated sample at each desired temperature point, typically within 2–50 °C. Control experiments with water *versus* water, buffer *versus* buffer and buffer *versus* water were performed for the evaluation of the absolute coefficient of thermal expansion, α_V, of the lipid phase.

High performance liquid chromatography (HPLC)

HPLC samples were analyzed utilizing an Ultimate 3000 HPLC System (Thermo Fisher Scientific GmbH, Dreieich, Germany) equipped with a quaternary pump (LPG-3400SD), an autosampler (WPS-3000TSL), a column compartment (TCC-3000SD), a diode array detector (DAD-3000), and a charged aerosol detector (Dionex Corona CAD; Dionex Softron GmbH, Germering, Germany). The flow rate was set to 1 mL min^{-1} and the autosampler was maintained at 20 °C. For all samples, a fixed injection volume of 10 μL was used. A reversed phase Luna C18(2) column (150 × 4.6 mm) with a particle size of 3 μm from Phenomenex Ltd (Aschaffenburg, Germany) was used for separation, which was kept at 45 °C. Separation was achieved using an isocratic eluent composition of 2% eluent A (4 mM ammonium acetate, pH 4.0) and 98% eluent B (4 mM ammonium acetate in methanol), with a total run duration of 15 minutes. The CAD detector employed for lipid quantification was operated with an inlet pressure of 35 psi, an evaporation temperature of 30 °C (factory fixed), a data acquisition rate of 10 Hz, and a maximum detection limit of 500 pA. The eluents were freshly prepared before usage. The HPLC system was equilibrated for a minimum of 20 minutes followed by two blank runs prior to sample analysis. Data evaluation was performed using Chromeleon® Software 7.2.1. The method was validated in accordance with the ICH guideline Q2(R2) addressing working range, precision, accuracy, detection limit, quantitation limit, and specificity.[46] Sample preparation was performed by diluting the original sample in ethanol. The samples were analyzed in triplicates. For further details, see ESI, Section 1.†

Asymmetric flow field flow fractionation (AF4) and multi-angle light scattering (MALS)

Daughter vesicles (DVs) and mother vesicles (MVs) were separated using AF4 as published elsewhere.[10] In brief, the AF4 setup consisted of a separation channel

(SC channel, regenerated cellulose membrane, cut-off 10 kDa, 490 μm spacer, wide type, Wyatt, Dernbach, Germany) and a flow controller (Eclipse AF4, Wyatt) connected online to MALS (DAWN Heleos II, Wyatt) and fluorescence (1260 Infinity G1321B, Agilent, Waldbronn, Germany) detectors. Separation buffer (110 mM NaCl, 10 mM Tris, 0.5 mM EDTA, and 0.02% NaN_3) was adjusted to pH 7.4 and filtered through 0.1 μm pores. Channel flow rate was set to 1.0 mL min^{-1} and 5–10 μg lipid sample was injected (0.2 mL min^{-1}). For separations at room temperature (RT; 23 ± 2 °C), the following AF4 sequence was used (cross flow rate $V_x = 0.08$ mL min^{-1} unless stated otherwise): (a) elution, 2 min; (b) focus, 2 min – focus + inject, 4 min – focus, 4 min; (c) elution, 20 min – elution, 23 min (linear V_x gradient: 0.80 to 0.05 mL min^{-1}) – elution, 15 min (V_x = 0.05 mL min^{-1}); (d) elution + inject, 5 min ($V_x = 0.0$ mL min^{-1}); (e) focus, 2 min – elution, 2 min. For separations at 4 °C, the same sequence was used with lower cross-flow rates (0.50 instead of 0.80 mL min^{-1} and 0.03 instead of 0.05 mL min^{-1}) to arrive at comparable retention times for a given sample at 23 °C and 4 °C. The geometric size of the vesicles was obtained from MALS data using the coated spheres model in ASTRA 8.0.1.21 (Wyatt). The fraction of fluorescence originating from the DVs was obtained from the fluorescence signal (λ_{ex} = 460 nm, λ_{ex} = 520 nm) as described earlier.[10]

Cryo-transmission electron microscopy (cryo-TEM)

Cryo-TEM samples were incubated 30 min at 35 °C before blotting. Then, 4 μL of liposomes at 6 mg mL^{-1} total lipid were deposited on a Quantifoil S 7/2 copper grid (Quantifoil, Jena, Germany). The grid was glow discharged using the PELCO easiGlow (Ted Pella, Redding, California, USA) immediately prior to use. The grid was blotted at 33 °C and 100% relative humidity and vitrified by plunge freezing into liquid ethane using a Vitrobot MK IV (ThermoFisher, Waltham, Massachusetts, USA). Imaging was performed under cryogenic conditions on a FEI Talos L120C at 120 kV operating voltage equipped with a Ceta 16-megapixel camera.

Results

Phase behavior in symmetrical LUVs of SOPC and DPPG

Usually, a thermodynamic assessment of lipid phase behavior is done with multilamellar vesicles, which fulfill the cooperativity requirements for true phases to a rather good approximation. The present study deals with aLUVs and, therefore, needs to record the state of the membranes in LUVs although their transitions are known to be broadened and deviate from the rules applying to true phases.

As a consequence, Fig. 1B obtained by DSC downscans for symmetric SOPC/DPPG LUVs (Fig. 1A) should not be referred to as a "phase diagram" but has been presented analogously. Fig. 1 represents an isomorphous melting behavior, *i.e.*, mixing of the lipids both in gel and fluid phase. Bold lines represent empirical approximations of effective solidus and liquidus boundaries, taking into account that phase boundaries must meet in a single T_m for pure components. Blue dash–dot lines illustrate the boundaries expected for ideal mixing of SOPC and DPPG in both phases, as calculated on the basis of the respective T_m and ΔH values. The deviations of the real boundaries can be explained by non-ideal mixing of the

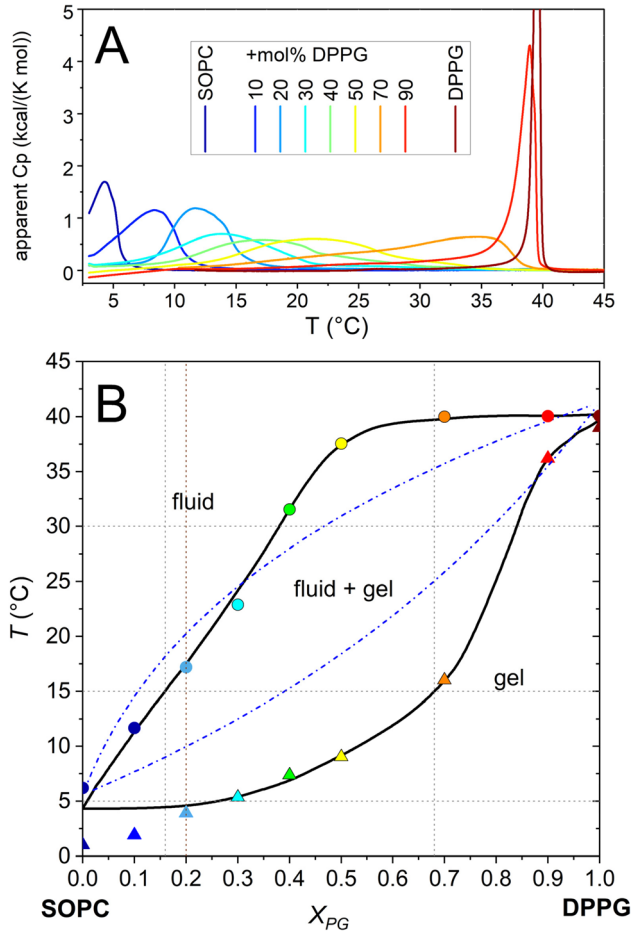

Fig. 1 Representation of the gel-to-fluid transition ranges in mixtures of SOPC and DPPG (panel A) presented analogously to a phase diagram (panel B). Temperatures at the onset (triangles) and completion (spheres) of transitions recorded by DSC at pH 7.4 are plotted as a function of the mole fraction of DPPG, X_{PG}, in symmetrical LUVs. The arbitrarily chosen, bold solid line would fulfill the requirements of a phase coexistence. Phase boundaries simulated for ideal mixing and high cooperativity (expected rather for MLV) are shown as dotted lines.

lipids (also seen in MLV phase diagrams) and compromised cooperativity and curvature effects in LUVs.

The calculations below were carried out interpreting the bold, arbitrary lines in Fig. 1B as approximations for true phase boundaries. Most important for the current study is the state of pure SOPC and SOPC with ~20 mol% DPPG at 5, 15, and 30 °C. The fraction of gel phase, x_{gel}, in pure SOPC is about 50% at 5 °C (close to T_m); at 15 and 30 °C, the membrane is all fluid. SOPC with 20 mol% DPPG (see vertical grid line) is fully fluid at 30 °C. At 15 °C, there is a coexistence of a gel phase with 68 mol% DPPG and a fluid phase with 16 mol% DPPG. The lever rule implies that the gel phase comprises $x_{gel} = (68 - 20)/(68 - 16) = 8$ mol% of the lipid; the remaining 92% is in the fluid phase. At 5 °C, the non-ideal behavior

permits only a rather crude estimate. DPPG contents of gel and fluid phase of 28 and 2 mol%, respectively, suggest $x_{gel} \approx 70$ mol%. These data will be used below to assess the intrinsic states of the leaflets in asymmetric liposomes.

The exchange protocol yields aLUVs also in partial gel state, at 5 and 15 °C

The exchange protocol established to yield aLUVs of POPC^{in}|+20 mol% POPG^{out} upon 20 minutes exchange at 28 °C[37,38] was applied to SOPC^{in}|+DPPG^{out} at 30 °C, 15 °C, and 5 °C.

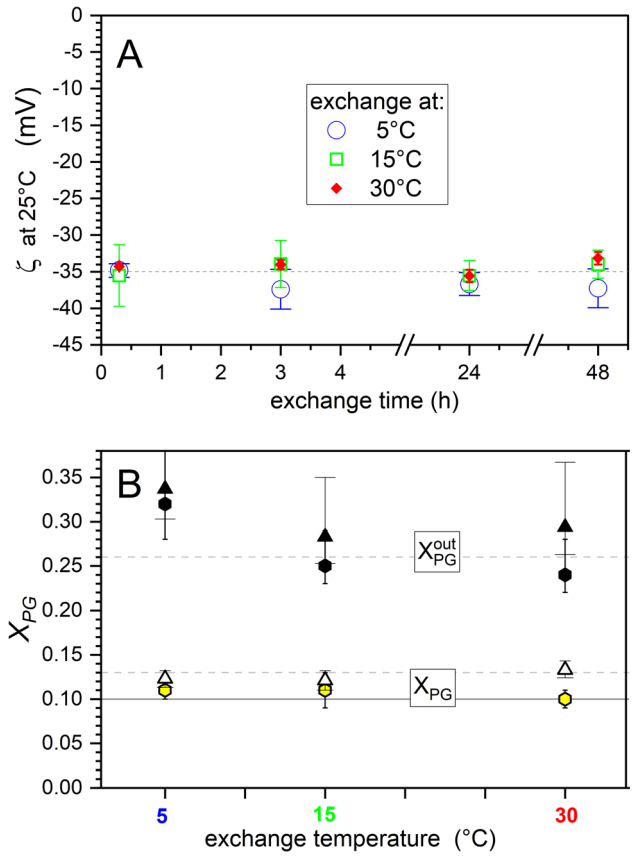

Fig. 2 Properties of aLUVs of SOPC^{in}|+20 mol% DPPG^{out} prepared by exchange between SOPC "acceptor" vesicles with nearly DPPG-saturated mβCD solution as a function of exchange time (A) and exchange temperature (B). Panel A shows data of batch 5 (see Table S8† for detailed data) as a function of exchange temperature (see plot) and exchange time (abscissa). The zeta potential, ζ, is related to the DPPG-based charge density in the outer leaflet; it is always measured at 25 °C to eliminate effects of varying membrane area. Panel B displays total DPPG mole fractions, X_{PG}, obtained using Fig. S3† from ζ of scrambled aLUVs (open triangles, batch 4) and HPLC (yellow hexagons, batches 1–3). PG mole fractions in the outer leaflet of aLUVs, X_{PG}^{out}, are obtained from ζ for batch 4 (solid black triangles) and batches 1–3 (solid black hexagons). Errors of HPLC-based data are s.d. of triplicate measurements. Errors of ζ-based data reflect lower and upper limits of the 95% confidence interval of the calibration curve, Fig. S3.†

The zeta potential of batch 5 (see Table S8† for details) reached −35 mV after 20 minutes of exchange at all temperatures, with larger errors at lower exchange temperatures (see Fig. 2A). It is related to the surface charge density. Since all ζ measurements are carried out at 25 °C, where all lipids are fluid and share a similar surface area, the charge density should represent the mole fraction of the charged species, DPPG, to a good approximation. Longer incubation times up to 48 h did not lead to any further uptake of DPPG into the outer leaflet at 15 and 30 °C; a slight trend at 5 °C is possible but lies within the rather large error range.

The total amount of DPPG inserted into liposomes was obtained from HPLC as 10–11 mol% and from ζ measurements of scrambled aLUVs as ∼12–14 mol% (Fig. 2B, open symbols); for raw data, see Table S8.† Conversion of the average ζ of 3 batches to X_{PG}^{out} was done by a calibration curve explained in Fig. S3.† The values obtained by the different methods are largely in line with each other and with the target value of 10% established for this protocol with POPC/POPG. The exchanged amount of DPPG did not significantly depend on exchange temperature. This is not trivial since cooling of mβCD–lipid complexes could induce supersaturation and the activity of DPPG in gel and fluid phase must be expected to be different.[13]

The ζ potential of aLUVs with all DPPG residing in the outer leaflet should correspond to twice the total DPPG content, $X_{PG}^{out} \approx 2X_{PG}$. Indeed, the experimental data (solid triangles for average of batches 1–3 and hexagons for batch 4 in Fig. 2B) are of the order of the upper dashed grid line at 26 mol%, twice that of the lower dashed grid line; again, the values are somewhat higher but mostly within error of the dashed line. As we will see below, samples prepared at 5 and 15 °C and then heated to room temperature show budding – we speculate that the coexistence of MV and DV with potentially different X_{PG}^{out} might cause minor deviations of ζ. In any case, the twofold higher X_{PG}^{out} compared to the average X_{PG} confirms the asymmetric insertion of DPPG, also at 5 °C and 15 °C exchange temperature.

Summarizing this section, the standard protocol established earlier applies also to prepare aLUVs of $SOPC^{in}$|+20% $DPPG^{out}$, even if the lipid is partially in the gel phase. The extent of DPPG insertion is quite similar to that of POPG.

Interleaflet coupling in aLUVs depends on exchange temperature

In order to gain information about interleaflet coupling in SOPC/DPPG liposomes, we studied the melting behavior in more detail using PPC, a calorimetric method that is capable of measuring the heat response to an isothermal pressure perturbation (see Fig. 3).

First, three replicate sets of aLUVs were prepared separately, one per set at an exchange temperature of 30 °C, followed by mβCD removal. This procedure is close to the standard one,[37,38] with both leaflets in the fluid phase. Each sample was cooled to 2 °C and several PPC runs carried out with temperature increasing from 2 °C to 45 °C, respectively. Unlike scanning calorimetry, in PPC, the calorimeter is equilibrated at each temperature point to be measured and then, down and up pressure jumps are applied to measure expansivity. Afterwards, the system heats to the next desired temperature. The PPC curves of the 3 replicate samples are presented as red lines in Fig. 3B, with their enclosed area filled with a red shading. A second plot of the data in a separate window and with detailed experimental points is provided as Fig. S5.† The width of the red area indicates some variability between the replicate aLUVs but overall, the curves agree in

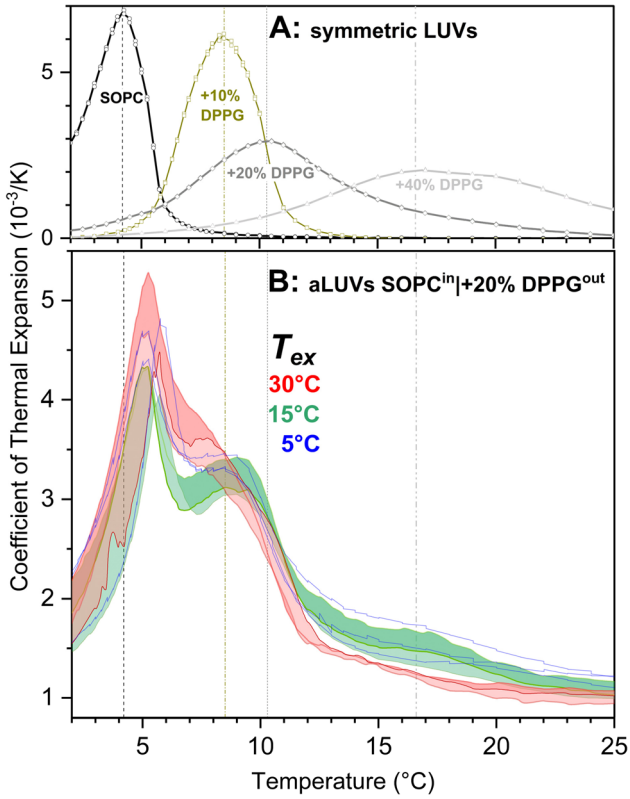

Fig. 3 PPC transition curves of aLUVs prepared at different exchange temperatures (B) compared to those of symmetric LUVs (A). For compositions, see plot (all percentages refer to mol%). In panel B, red curves enclosing a red area represent three replicate samples prepared at 30 °C exchange temperature. Green curves and green shading represent aLUVs prepared at 15 °C. aLUVs prepared at 5 °C are represented by blue curves (no shading). PPC transition curves can be interpreted analogously to DSC curves; here, the progress of the melting transition is indicated by a peak in thermal expansion instead of the – related – peak of apparent heat capacity detected by DSC. Panel B is focused on a general comparison – a repetition of all data with individual data points assigned to sample sets is provided as Fig. S5.†

showing a significant coupling. As discussed below, there is no standard way of quantifying interleaflet coupling from transition curves – our statement of "significant yet incomplete coupling" is based on two observations: first, the peak is considerable narrower and more overlapping than the superimposed transition curves of symmetric LUVs of SOPC (matching the composition of the inner leaflet) and SOPC + 20 mol% DPPG (as in outer leaflet) shown in Fig. 3A. This is taken as evidence for coupling. Second, the transition does not collapse into a single, homogeneous intermediate peak as, for example, that for symmetric LUVs with the average 10 mol% DPPG (Fig. 3A) but retains a sharp peak on the low-temperature side and a pronounced shoulder on the high-temperature side. This is interpreted in terms of incomplete coupling.

For each of the 3 sets of samples, there was also one sample with lipid exchange at 15 °C. Also these samples were measured in PPC starting at 2 °C,

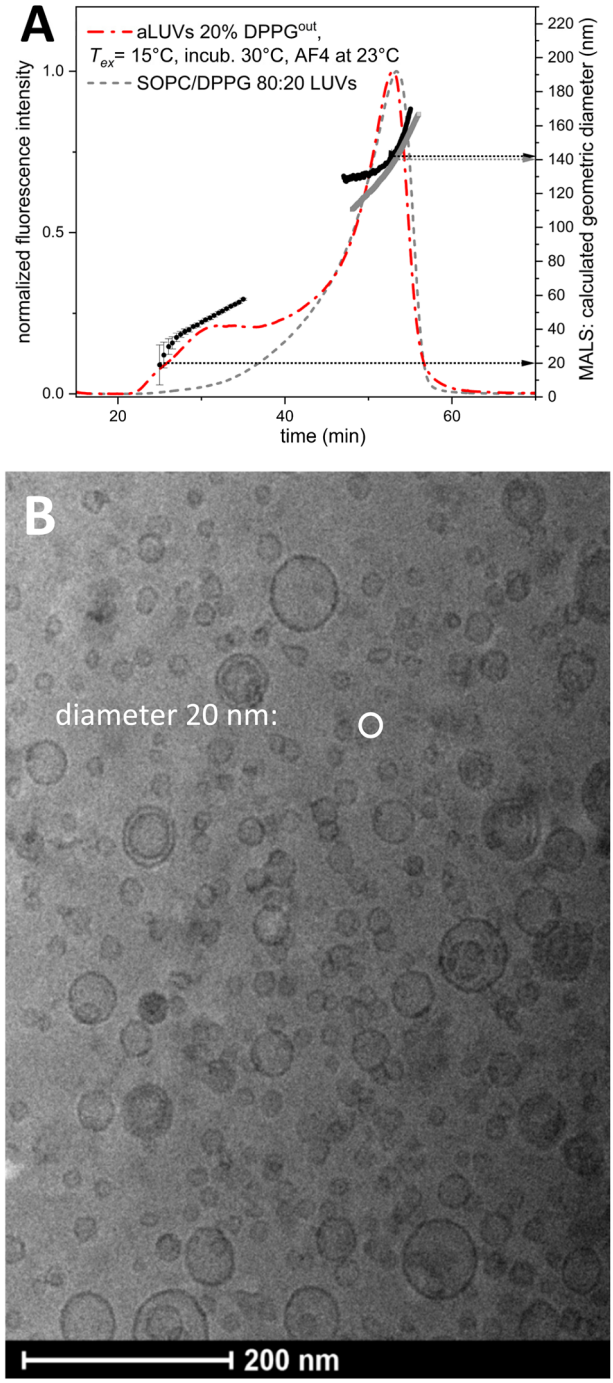

Fig. 4 Detection of small DVs in aLUV prepared at 15 °C after cyclodextrin removal and subsequent temperature increase as seen by AF4 (A) and cryo-transmission electron microscopy (cryo-TEM) (B). (A) The red dash–dot line (fluorescence signal, left axis) and black dots (MALS, right axis) represent a sample with 23 mol% DPPG in the outer leaflet after 30 min incubation at 35 °C, measured at 23 °C. The grey dashed curve (left axis) and

giving rise to the three green curves enclosing the green area in Fig. 3B (reproduced in detail in Fig. S5†). According to the criteria explained above, the transitions are rated to show significant but weaker coupling than that seen for the 30 °C-exchanged aLUVs. The two peaks of the green curves are farther apart and better separated than the shoulders of the red ones. Three samples prepared at 5 °C yielded the blue curves (see also Fig. S5†). For better visibility, no shading was done. The curves are largely within the green shading, indicating that there was no significant difference between the transitions of the aLUVs prepared at 5 and 15 °C.

Detecting budding of DVs after exposing aLUVs to temperature changes

Fig. 4 shows the typical AF4 elution profiles of symmetric LUVs (grey dashed curve) and of aLUVs produced at an exchange temperature of 15 °C ($T_{ex} = 15$ °C) and, after cyclodextrin removal, heated up to 35 °C and measured at 23 °C (red, dash–dot curve). The shoulder of the aLUV profile at short elution times implies the presence of a substantial number of much smaller particles. MALS data of the same run (black spheres, right axis) imply sizes of the order of 20 nm and somewhat larger at the shoulder. Symmetrical liposomes and remaining large aLUV show a peak size of ~140 nm.

The nature of the small particles created from aLUVs is clarified by cryo-TEM. Fig. 4B shows a large number of vesicles with diameters around 20 nm that illustrate and confirm the AF4 result. Note that the cryo-TEM picture displays DV sizes by number. The fluorescence signal (see red dash–dot line in Fig. 4A) corresponding to a given particle size scales with the fluorophore content of the vesicle, which increases with vesicle area, *i.e.*, the second power of size. Therefore, the local maximum of fluorescence seen for ~40 nm is not in conflict with a majority of DVs being in the 20 nm range.

The disagreement of the grey and black MALS curves in Fig. 4A illustrates that there is no strictly conserved correlation between size and elution time in the AF4 system. It is therefore important to consider MALS and fluorescence data in parallel for a given AF4 run.

Overall, Fig. 4B supports the interpretation of a short-time shoulder of AF4 profiles as shown here in terms of the presence of very small DVs, in line with previous results on lysolipid-induced budding of DVs.[10,16]

The question arises under which conditions such DVs appear and whether their formation is reversible. Fig. 5 shows AF4 elution profiles of aLUVs prepared at different exchange temperatures after cyclodextrin removal. The solid lines represent the first run, still at or somewhat below exchange temperature. These profiles are similar to those for symmetric liposomes (Fig. 4).

After incubating the aLUVs prepared at T_{ex} of 5 and 15 °C at 35 °C for 30 min, aliquots were taken again for AF4 carried out at 23 °C (red dash–dot lines in panels A and B). They show a pronounced shoulder assigned above to the appearance of small DVs with diameters of the order of 20 nm. The dashed curves in Fig. 5A and B were obtained by a third AF4 test of the samples after cooling

grey squares (right axis) were obtained with symmetrical LUVs of SOPC with 20% DPPG overall. (B) Cryo-TEM of sample treated analogously to aLUVs in (A), with specific DPPG content of 29 mol% in the outer leaflet according to ζ.

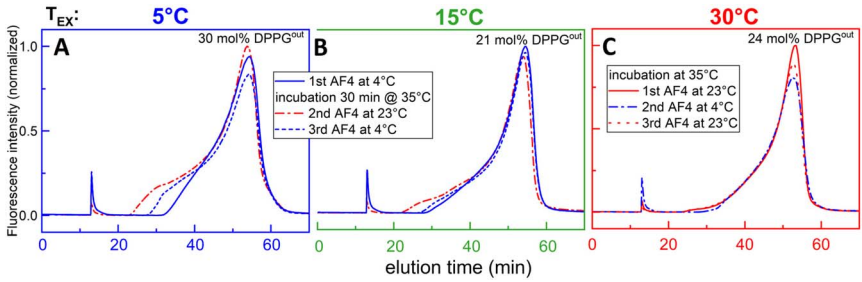

Fig. 5 AF4 elution profiles of aLUVs still at lipid-exchange temperature (solid lines), after incubation at different temperature (dash–dot) and back to T_{ex} (dashed) – line colors indicate AF4 temperatures of 4 °C (blue) or 23 °C (red). The different panels correspond to different exchange temperatures as marked in the plot. Zeta potential data yielded outer leaflet contents of DPPG of 21–30 mol% in SOPC vesicles, as indicated in the plots. Note that the first peak at 12 min is a technical artefact.

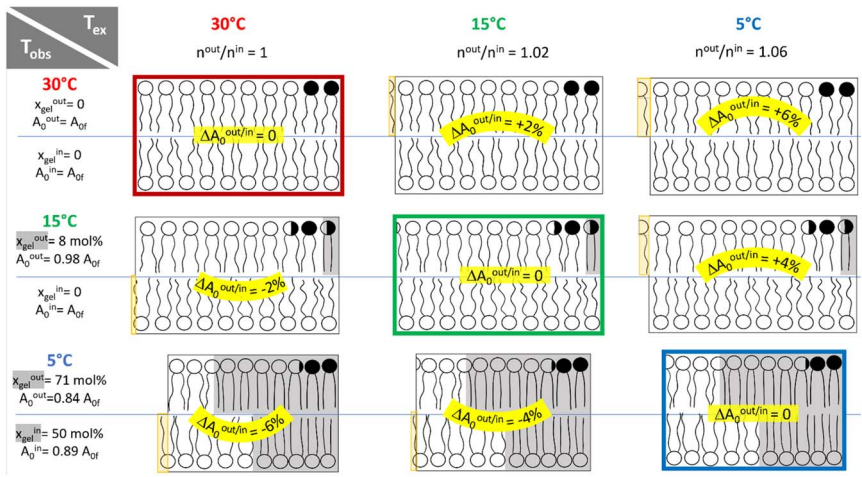

Fig. 6 Semiquantitative illustration of the model assuming negligible intrinsic area mismatch (*i.e.*, asymmetry stress), $\Delta A_0^{out/in} = 0$, at the exchange temperature, T_{ex}, at which aLUVs were prepared by equilibration with nearly lipid-saturated cyclodextrin. Columns of boxes represent selected exchange temperatures, rows temperatures of observation after cyclodextrin removal, T_{obs}. Note that the population number of the two leaflets, n^{out}/n^{in}, is conserved for a given T_{ex} (column) whereas the intrinsic fraction of gel phase, x_{gel}, and in turn, the average intrinsic area, A_0, for a given leaflet depends on observation temperature, T_{obs}. Temperature-induced intrinsic-area mismatch causes asymmetry stress and a tendency to bend the bilayer as indicated schematically.

them back down to 4 °C. The intermediate position of the shoulder between original (blue, first run) and budded (red, second run) state implies that DVs budding has been partially reversible; *i.e.*, some DVs seem to fuse upon cooling back.

The aLUVs produced at $T_{ex} = 30$ °C (Fig. 5C) do not show DVs, neither originally nor after cooling or re-heating. Summarizing, the appearance of small

exovesicles is seen only for aLUVs prepared at 5 and 15 °C and then heated up to ≥23 °C.

Discussion

The hypothesis of "conserved intrinsic area upon exchange"

Baumgart and coworkers[13] showed for the exchange of lipid between lipid-loaded cyclodextrin and the outer leaflet of "acceptor" liposomes that there is a "crossing" lipid load of cyclodextrin. At lower loading, cyclodextrin tends to extract lipid from membranes. Lipid-supersaturated cyclodextrin inserts additional lipid into acceptor liposomes. To some extent, this consequence of an equilibrium distribution of the lipid is analogous to the cyclodextrin–vesicle partitioning of cholesterol.[47] The principal difference is that cholesterol equilibrates quickly between the leaflets and can be supplied or extracted quasi-symmetrically. Insertion *versus* removal of lipid from GUVs has been characterized by comparing the occurrence of invaginations or inward tubulation induced by outer-leaflet depletion with that of exvagination driven by overpopulation of the outer leaflet.[13]

Previous work[37,38] has shown that exchange of outer-leaflet POPC with POPG added in the form of cyclodextrin–lipid complexes replaces one POPC by one POPG as long as the added cyclodextrin is loaded with POPG close to saturation. There was no preference for one lipid over the other so that the PG : PC mole ratio in the outer leaflet after exchange agreed with that in the cyclodextrin complexes in solution and hence, with the total ratio between added DPPG and outer-leaflet POPC prior to exchange.

Importantly, the apparent saturation of cyclodextrin with lipid results from a high dissociation constant[13,37] and not from a full, stoichiometric binding; >90% of mβCD does not carry lipid. This renders the chemical potential of the complex little dependent on concentration. Over a finite range in cyclodextrin concentration, it simply absorbs the lipid that supersedes the intrinsic area of the outer leaflet and provides the lipid to fill the outer leaflet to match intrinsic and real area. Only well below saturation, cyclodextrin provides less lipid than extracting so that the outer leaflet becomes underpopulated[13] and ultimately, liposomes get dissolved.[13,37,48]

Defining a relative intrinsic-area mismatch, $\Delta A_0^{\mathrm{out/in}}$:

$$\Delta A_0^{\mathrm{out/in}} = \frac{2\left(n^{\mathrm{out}} A_0^{\mathrm{out}} - n^{\mathrm{in}} A_0^{\mathrm{in}}\right)}{n^{\mathrm{out}} A_0^{\mathrm{out}} + n^{\mathrm{in}} A_0^{\mathrm{in}}} \quad (1)$$

our hypothesis implies that upon proper exchange $\Delta A_0^{\mathrm{out/in}} \approx 0$. Here, n stands for the number of lipid molecules in a given bilayer – setting $n^{\mathrm{in}} = 1$, n^{out} simply becomes the number of outside lipids per inside lipid. A_0^{in} and A_0^{out} stand for the average intrinsic interfacial area per molecule in the inner and outer leaflet, respectively.

Let us, first, estimate A_0^{in} and A_0^{out} as a function of temperature. In the text concerning Fig. 1 above, we have estimated the intrinsic fraction of gel phase for SOPC forming the inner leaflet, $x_{\mathrm{gel}}^{\mathrm{in}}$, to be 50% at 5 °C and zero at ≥15 °C. For 20 mol% DPPG in SOPC, a typical composition of the outer leaflet, we obtained $x_{\mathrm{gel}}^{\mathrm{out}}$ of 71, 8 and 0 mol% at 5, 15 and 30 °C, respectively. Intrinsic fraction means here that the leaflet can form the phase that would be formed by a bilayer of the

same composition and area per molecule, *i.e.*, it excludes coupling to a different leaflet.

The fraction x_{gel} governs A_0 because lipids shrink substantially upon freezing to the gel phase. For DPPG, $A_0 \approx 61$ Å^2 in the fluid[49] and 47 Å^2 in the gel[50,51] phase (for an overview, see Marsh[40]); *i.e.*, freezing reduces the area by a factor of 0.77. For simplicity and in lack of data for SOPC in the gel, we will assume for the semi-quantitative discussion here that both lipids have the same intrinsic areas of A_{0f} in the fluid and $A_{0gel} \approx 0.77A_{0f}$ in the gel phase. Then, A_0 becomes

$$\begin{aligned} A_0 &= A_{0f}\left(1 - x_{gel}\right) + A_{0gel}x_{gel} \\ &\approx A_{0f}\left(1 - 0.23x_{gel}\right) \end{aligned} \tag{2}$$

Lateral thermal expansion within the gel and fluid phase are neglected. With eqn (2) and the x_{gel} estimates given in the previous paragraph, one obtains the A_0 values for selected observation temperatures as provided in the left column of Fig. 6.

The upper left box in Fig. 6 illustrates aLUVs with 20 mol% DPPG^{out} that have been prepared at an exchange temperature of 30 °C, then separated from (partially lipid-loaded) cyclodextrin, incubated at 35 °C and finally characterized by AF4 at 23 °C. The DPPG content has been established maintaining a $\Delta A_0^{out/in}$ of zero – in line with our model – by exchanging 2 out of ten fluid SOPC with fluid DPPG. As the cyclodextrin has been removed, the lipids are fixed in their leaflets and the ratio $n^{out}/n^{in} = 1$ is conserved, independently of the observation temperature (first column in Fig. 6). If this sample is now cooled to 15 °C (one row down in Fig. 6), an intrinsic area mismatch is created by the freezing of 8 mol% of the outer leaflet lipid to the gel phase. Eqn (1) yields $\Delta A_0^{out/in} = 2 \times (0.98 - 1)/(0.98 + 1) = -2\%$, a negative stress that should favor a convex, inward bending. Cooling further to 5 °C yields, with the A_0^{out} and A_0^{in} shown on the left side, a mismatch of −6%.

The second column of boxes refers to aLUVs produced by exchange at 15 °C. As discussed in the previous paragraph, gel formation in the outer leaflet causes a shrinking of the average area per lipid by 2%. Then, the assumption of $\Delta A_0^{out/in}$ to be 0 as long as almost-lipid-saturated cyclodextrin is present implies that the outer leaflet contains a factor $n^{out}/n^{in} = 1.02$ times more lipid molecules. Again, this ratio is fixed as the cyclodextrin is removed and temperature-dependent changes in A_0^{out} and A_0^{in} cause intrinsic area mismatches that are positive, *i.e.*, outward-bending upon temperature increase and negative upon cooling. The same procedure yields a lipid number overpopulation of $n^{out}/n^{in} \approx 1.06$ for exchange at 5 °C and subsequent, positive intrinsic area mismatches at higher observation temperature.

Summarizing, the data support the concept that heating up aLUVs prepared under conditions of ordered outer and disordered inner (OO/DI) leaflets causes exovesiculation of small DVs upon OO melting. The underlying rationale predicts the same effect for aLUVs prepared in the all-fluid state and then cooled to a DO/OI scenario, *i.e.*, with lipid freezing in the inner leaflet.

In the literature, a number of such OO/DI systems have been studied without specifically addressing a potential DV budding. As discussed, spot checks with cryo-TEM can hardly provide a detailed assessment of budding but Fig. 3B of Eicher *et al.*[26] presents pictures of POPE^{in}|POPC^{out} that resemble our Fig. 4B. In this system, exovesiculation would be favored both by the shrinking of the inner

leaflet upon POPE freezing and by the negative intrinsic curvature of the inner leaflet that would stabilize the strongly curved inner leaflet of a DV.

Budding as an alternative to asymmetry-stress-induced coupling?

In the introduction, we have mentioned a considerable number of interleaflet coupling mechanisms discussed in the literature. Here, we propose the interplay between intrinsic-area asymmetry and budding to be an additional coupling (or de-coupling) mechanism. Experimentally, the introduction of AF4 enabled us to sensitively detect exovesiculation (outward budding); we are not aware of information regarding inward budding from aLUVs. Whereas GUVs are free to bud cylindrical or other highly curved structures with microscopic dimensions to either side,[13] this may be different for LUVs. Scaling vesicles down by more than one order of magnitude brings sizes of DVs (or other budding structures) toward the order of membrane thickness. It should then matter whether budding proceeds towards or against the original curvature of the bilayer. Even if inward budding from LUVs can proceed, it would be limited to a smaller fraction of lipid than outward budding. The limit arises from the fact that small DVs have a larger surface-to-volume ratio than the original, large vesicle so that budding uses up excess area "stored" in deviations from spherical shape.[10,13] As mother vesicles become increasingly spherical, budding becomes increasingly opposed and stops. Inward DVs need even more membrane surface since their volume is enclosed by two bilayers.

Our data can, qualitatively, be explained on the basis of the "either coupling or (outward) budding" hypothesis. aLUVs prepared at 30 °C show no exovesiculation and increased interleaflet coupling of the melting transitions. Those prepared at 5 and 15 °C cause budding upon lipid melting and comparably weaker coupling. This is what one should expect if the other coupling mechanisms described play no major role here and inward budding is not or less possible.

aLUVs of POPC and the higher-melting POPE studied by Eicher *et al.*[26] do not support our simple "either coupling or budding" hypothesis. The fact that $POPE^{in}|+POPC^{out}$ shows strong coupling of the melting transition, but $POPC^{in}|+POPE^{out}$ does not, has been explained on the basis of the negative intrinsic curvature of POPE. From the perspective of intrinsic-area asymmetry, the question arises why the $POPE^{in}|+POPC^{out}$ system, which might develop positive ΔA_0 and do outward budding, is coupling anyway. As mentioned, budding is limited by the available excess area.[10,13] The maximal intrinsic-area asymmetry in this system is quite high; at ~12–20 °C, the intrinsic state of the outer leaflet is virtually all fluid and the inner all gel,[26] causing a $\Delta A_0 \approx +26\%$. Hence, there might be some budding but this might not suffice to eliminate coupling. The reverse aLUVs, $POPC^{in}|+POPE^{out}$, should develop a highly negative ΔA_0 which cannot be relaxed by outward budding. The finding that the transitions in the leaflets are hardly coupled points to some unknown pathway how this ΔA_0 is accommodated, with inward budding being a principal option to be explored.

A paper preparing $POPC^{in}|+DPPC^{out}$ at room temperature and studying the sample at 55 °C, *i.e.*, likely undergoing $o \rightarrow d^{in}|d^{out}$ as in our study, does not seem to provide evidence suggesting or excluding budding.[19] It shows weak coupling. Other publications dealt with possible $d^{in}|d \rightarrow o^{out}$ scenarios[24,26,36,52–54] that are expected to induce negative ΔA_0. The respective papers report both strong and

weak coupling for the different systems. A table compiling information about interleaflet coupling in aLUVs is provided as Table S9.†

Overall, there are sophisticated models describing coupling as such[30,55,56] but a prediction of the extent of coupling for a given combination of leaflet compositions and preparation conditions is still lacking. It is mechanistically convincing that asymmetry stress is a coupling mechanism that can be inhibited by budding. However, this neither excludes budding to happen in addition to coupling nor weak or no coupling to be found although budding is impossible or unlikely.

The problem of quantifying coupling

Another problem is that there is no clear-cut way to quantify the extent of coupling of phase transitions. Weak or no coupling is indicated by a thermotropic transition curve resembling a simple superposition of individual transitions. A good example[26] for weak coupling following this criterion is $POPC^{in}|+POPE^{out}$.

One model for a transition curve of aLUVs with strong coupling is that of the corresponding scrambled vesicles or of separately prepared, symmetric LUVs with the same overall composition. In Fig. 1B, we provide such a symmetrical analog curve measured with SOPC + 10 mol% DPPG symmetrically to model perfect coupling of aLUV with $SOPC^{in}|+20$ mol% $DPPG^{out}$. The agreement is poor, arguing against strong coupling. In contrast, aLUV data of $POPE^{in}|+POPC^{out}$ agreed quite well with their symmetrical analog,[26] indicating strong coupling.

It should, however, be noted that the model that a DSC curve of strong coupling resembles that of a scrambled sample is not unequivocal. Furthermore, the idea of "intermediate coupling" to give rise to transition curves with peaks in between those of averaged and scrambled-lipid curves is not trivial. Cheng and London[24] measured the fluorescence anisotropy of DPH and TMA-DPH in aLUVs of $DOPE\text{-}POPS^{in}|+SM^{out}$. The temperature-dependent steady-state anisotropy of DPH for these aLUVs was compared with those of symmetrical LUVs of the compositions of the inner, the outer, and scrambled leaflets. The resulting curves for averaged (not explicitly shown) and scrambled-like vesicles were, in fact, not much different from each other. Importantly, the experimental data for aLUVs were not at or in between these model curves but much closer to that for the SM-rich, outer leaflet. Assuming that DPH remained homogeneously distributed between the leaflets and showed about the same fluorescence lifetimes there, this argues for a strongly non-ideal mixing in the gel phase. In such a non-ideal system, it seems non-trivial to assess the extent of coupling in the first place.

Technical and biological implications of asymmetric transitions

Above, it has been demonstrated that the structural and thermodynamic properties of aLUVs depend on the specific conditions upon preparation such as the exchange temperature. Furthermore, potentially irreversible processes such as budding and fission of DVs render an aLUV sample dependent on its thermal history; storing an aLUV sample in the fridge might change it substantially.

The potential importance of interleaflet coupling for transmembrane signaling has long been recognized. An interesting aspect in this regard is the finding that the budding of DVs is partially reversible. That means that very small vesicles become fusogenic when their intrinsic-area asymmetry ΔA_0 decreases by a shrinking of the outer or expansion of the inner leaflet. This may also modulate the activity of

protein-based remodeling machineries. Maiti and coworkers[57] have demonstrated that the SNARE-driven fusion of synaptic vesicles is promoted by a high serotonin content. Inner leaflet expansion by intercalating amphiphilic serotonin molecules should, indeed, cause a reduction of ΔA_0. Cell membranes with asymmetric order–disorder transitions have to regulate their intrinsic area asymmetry to avoid strong temperature dependencies of membrane remodeling processes.

Conclusions

The preparation of aLUVs *via* lipid exchange with cyclodextrin complexes works also in the gel phase. Mixing of DPPG and SOPC between cyclodextrin and aLUVs remained at least close to random.

The data are in line with the hypothesis that lipid exchange between aLUV outer leaflets and cyclodextrin loaded with another lipid close to saturation produces largely asymmetry-stress-free liposomes. This explains also the finding that aLUVs differ in their properties depending on the exchange temperature they have been prepared at.

Our data support the "coupling or budding" hypothesis that intrinsic-area asymmetry changes should impose interleaflet coupling of asymmetric melting or freezing transitions unless it can be accommodated by the budding and fission of daughter vesicles (DVs). However, published data are not in line with this simple idea – highlighting the complexity of coupling phenomena. A prediction of the extent of coupling based on leaflet compositions and preparation procedure remains impossible so far.

Partial reversibility of DV budding demonstrates that small vesicles can be rendered fusogenic as their intrinsic-area asymmetry is reduced.

Data availability

The data supporting this article are included as part of the supplementary information.†

Author contributions

H. H. conceived the study. M. K. coordinated the work and designed, carried out and analyzed DSC, PPC, DLS and most AF4 experiments. M. J. and M. K. established and applied the HPLC protocol. S. G. contributed some AF4 experiments; M. H. supported AF4 and established the AF4 setup at 5 °C. J. L. and L. K. did the cryo-TEM. H. H. supervised the experiments. M. K. wrote the first draft with assistance from other authors; all authors discussed and edited the draft and H. H. and M. K. finalized the manuscript. All authors approved the final version.

Conflicts of interest

The authors declare having no conflicts of interest.

Acknowledgements

Major instrumentation was funded by the Center for Biological Signaling Studies, BIOSS. S. G. acknowledges funding from the Deutsche Forschungsgemeinschaft (DFG, German Research Foundation) *via* the Research Training Group 2202 "Transport into and across membranes" (278002225/RTG 2202). We thank Lipoid GmbH (Ludwigshafen, Germany) for providing the lipids. The authors thank A. Meister, G. Pabst, T. Gutsmann, and D. Huster for constructive discussions.

References

1 J. Israelachvili, *Intermolecular and surface forces*, Academic Press, Amsterdam, 1984.
2 R. A. Demel and B. De Kruyff, *Biochim. Biophys. Acta, Rev. Biomembr.*, 1976, **457**, 109–132.
3 P. L. Yeagle, *Biochim. Biophys. Acta, Rev. Biomembr.*, 1985, **822**, 267–287.
4 H. Heerklotz and A. Tsamaloukas, *Biophys. J.*, 2006, **91**, 600–607.
5 S. M. Gruner, *Proc. Natl. Acad. Sci. U. S. A.*, 1985, **82**, 3665–3669.
6 M. P. Sheetz and S. J. Singer, *Proc. Natl. Acad. Sci. U. S. A.*, 1974, **71**, 4457–4461.
7 J. Steigenberger, Y. Verleysen, N. Geudens, J. C. Martins and H. Heerklotz, *Front. Microbiol.*, 2021, **12**, 2644.
8 H. Heerklotz and J. Seelig, *Eur. Biophys. J.*, 2007, **36**, 305–314.
9 H. Y. Fan, D. Das and H. Heerklotz, *Langmuir*, 2016, **32**, 11655–11663.
10 L. Hua, M. Kaiser, I. Carabadjac, A. Meister, G. Hause and H. Heerklotz, *Biophys. J.*, 2023, **122**, 4011–4022.
11 H. Y. Fan and H. Heerklotz, *J. Colloid Interface Sci.*, 2017, **504**, 283–293.
12 U. Kragh-Hansen, M. Le Maire and J. V. Møller, *Biophys. J.*, 1998, **75**, 2932–2946.
13 T. Reagle, Y. Xie, Z. Li, W. Carnero and T. Baumgart, *Soft Matter*, 2024, **20**, 4291–4307.
14 V. N. Georgiev, A. Grafmüller, D. Bléger, S. Hecht, S. Kunstmann, S. Barbirz, R. Lipowsky and R. Dimova, *Adv. Sci.*, 2018, **5**, 1800432.
15 S. Penič, L. Mesarec, M. Fošnarič, L. Mrówczyńska, H. Hägerstrand, V. Kralj-Iglič and A. Iglič, *Front. Phys.*, 2020, **8**, 342, DOI: **10.3389/fphy.2020.00342**.
16 L. Hua, S. Akcesme, K. Müller and H. Heerklotz, *J. Phys. Chem. B*, 2025, **129**, 1260–1273.
17 H. Heerklotz, *Biophys. J.*, 2001, **81**, 184–195.
18 R. Jin and T. Baumgart, *Soft Matter*, 2021, **17**, 7506–7515.
19 F. A. Heberle, D. Marquardt, M. Doktorova, B. Geier, R. F. Standaert, P. Heftberger, B. Kollmitzer, J. D. Nickels, R. A. Dick, G. W. Feigenson, J. Katsaras, E. London and G. Pabst, *Langmuir*, 2016, **32**, 5195–5200.
20 B. Eicher, F. A. Heberle, D. Marquardt, G. N. Rechberger, J. Katsaras and G. Pabst, *J. Appl. Crystallogr.*, 2017, **50**, 419–429.
21 L. Dietel, L. Kalie and H. Heerklotz, *Biophys. J.*, 2020, **119**, 767–779.
22 J. Steigenberger, Y. Verleysen, N. Geudens, J. C. Martins and H. Heerklotz, *Front. Microbiol.*, 2021, **12**, 669709, DOI: **10.3389/fmicb.2021.669709**.
23 U. Kragh-Hansen, M. Le Maire and J. V. Møller, *Biophys. J.*, 1998, **75**, 2932–2946.
24 H.-T. Cheng and E. London, *Biophys. J.*, 2011, **100**, 2671–2678.

25 G.-S. Yang, A. Wagenknecht-Wiesner, B. Yin, P. Suresh, E. London, B. A. Baird and N. Bag, *Biophys. J.*, 2024, **123**, 2256–2270.
26 B. Eicher, D. Marquardt, F. A. Heberle, I. Letofsky-Papst, G. N. Rechberger, M.-S. Appavou, J. Katsaras and G. Pabst, *Biophys. J.*, 2018, **114**, 146–157.
27 M. P. K. Frewein, P. Piller, E. F. Semeraro, O. Czakkel, Y. Gerelli, L. Porcar and G. Pabst, *Biophys. J.*, 2023, **122**, 2445–2455.
28 G. W. Feigenson, J. Huang and T. A. Enoki, *J. Am. Chem. Soc.*, 2023, **145**, 21717–21722.
29 V. Kiessling, C. Wan and L. K. Tamm, *Biochim. Biophys. Acta, Biomembr.*, 2009, **1788**, 64–71.
30 M. D. Collins and S. L. Keller, *Proc. Natl. Acad. Sci. U. S. A.*, 2008, **105**, 124–128.
31 T. R. Galimzyanov, R. J. Molotkovsky, M. E. Bozdaganyan, F. S. Cohen, P. Pohl and S. A. Akimov, *Phys. Rev. Lett.*, 2015, **115**, 088101, DOI: **10.1103/PhysRevLett.115.088101**.
32 A. Hossein and M. Deserno, *Biophys. J.*, 2020, **118**, 624–642.
33 J. D. Nickels, J. C. Smith and X. Cheng, *Chem. Phys. Lipids*, 2015, **192**, 87–99.
34 M. P. K. Frewein, P. Piller, E. F. Semeraro, K. C. Batchu, F. A. Heberle, H. L. Scott, Y. Gerelli, L. Porcar and G. Pabst, *J. Membr. Biol.*, 2022, **255**, 407–421.
35 T. A. Enoki and G. W. Feigenson, *Biochim. Biophys. Acta, Biomembr.*, 2022, **1864**, 183995.
36 S. Chiantia and E. London, *Biophys. J.*, 2012, **103**, 2311–2319.
37 M. Markones, C. Drechsler, M. Kaiser, L. Kalie, H. Heerklotz and S. Fiedler, *Langmuir*, 2018, **34**, 1999–2005.
38 M. Markones, A. Fippel, M. Kaiser, C. Drechsler, C. Hunte and H. Heerklotz, *Biophys. J.*, 2020, **118**, 294–302.
39 Y.-P. Zhang, R. N. A. H. Lewis and R. N. McElhaney, *Biophys. J.*, 1997, **72**, 779–793.
40 D. Marsh, *Handbook of Lipid Bilayers*, 2013.
41 M. J. Hope, M. B. Bally, G. Webb and P. R. Cullis, *Biochim. Biophys. Acta, Biomembr.*, 1985, **812**, 55–65.
42 R. C. MacDonald, R. I. MacDonald, B. P. M. Menco, K. Takeshita, N. K. Subbarao and L. Rong Hu, *Biochim. Biophys. Acta, Biomembr.*, 1991, **1061**, 297–303.
43 G. R. Bartlett, *J. Biol. Chem.*, 1959, **234**, 466–468.
44 V. V Plotnikov, J. M. Brandts, L. N. Lin and J. F. Brandts, *Anal. Biochem.*, 1997, **250**, 237–244.
45 H. Heerklotz and J. Seelig, *Biophys. J.*, 2002, **82**, 1445–1452.
46 European Medicines Agency, Validation of Analytical Procedures Q2(R2), Committee for Medicinal Products for Human Use EMA/CHMP/ICH/82072/2006, 2023, **https://database.ich.org/sites/default/files/ICH_Q2%28R2%29_Guideline_2023_1130.pdf**.
47 A. Tsamaloukas, H. Szadkowska, P. J. Slotte and H. Heerklotz, *Biophys. J.*, 2005, **89**, 1109–1119.
48 T. G. Anderson, A. Tan, P. Ganz and J. Seelig, *Biochemistry*, 2004, **43**, 2251–2261.
49 G. Pabst, S. L. Grage, S. Danner-Pongratz, W. Jing, A. S. Ulrich, A. Watts, K. Lohner and A. Hickel, *Biophys. J.*, 2008, **95**, 5779–5788.

50 A. Watts, K. Harlos and D. Marsh, *Biochim. Biophys. Acta, Biomembr.*, 1981, **645**, 91–96.
51 G. Pabst, S. Danner, S. Karmakar, G. Deutsch and V. A. Raghunathan, *Biophys. J.*, 2007, **93**, 513–525.
52 H.-T. Cheng and E. London, *J. Biol. Chem.*, 2009, **284**, 6079–6092.
53 S. Chiantia, P. Schwille, A. S. Klymchenko and E. London, *Biophys. J.*, 2011, **100**, L1–L3.
54 Q. Lin and E. London, *Biophys. J.*, 2015, **108**, 2212–2222.
55 S. May, *Soft Matter*, 2009, **5**, 3148–3156.
56 A. J. Wagner, S. Loew and S. May, *Biophys. J.*, 2007, **93**, 4268–4277.
57 D. Saha Roy, A. Gupta, V. Vishvakarma, P. Krupa, M. S. Li and S. Maiti, *J. Phys. Chem. B*, 2024, **128**, 4975–4985.

